

1 Identifying bovine respiratory disease infectious agents via
2 mechanistic modelling and symptomatic dynamics: application for
3 optimal pathogen-informed treatment interventions

4

5 Theophile Ghislain Loic EYANGO TABI^{a,b,c,*}, Halifa FARCHATI^a, Victoria POTDEVIN^b ,Xavier
6 L'HOSTIS^b, Nicolas PARISEY^c, Sébastien PICAULT^a

7

8 ^aOniris, INRAE, BIOEPAR, 44300, Nantes, France

9 ^bAdventiel, 7 boulevard Nominöé, 35740, Pacé, France

10 ^cINRAE, IGEPP, La motte au Vicomte, 35640, Le Rheu, France

11 *Corresponding author: loic.eyango@adventiel.fr

12

13

14

15 **Abstract (max 250 words)**

16

17 Bovine Respiratory Disease poses significant health and economic challenges in the cattle industry.
18 Mechanistic modelling offers a powerful alternative to understand BRD transmission and evaluate
19 the efficiency of various control strategies. In this study, we investigate three pathogen-specific
20 models representing the Orthopneumovirus bovis(BRSV), *Mannheimia haemolytica* (*Mh*), and
21 *Mycoplasmopsis bovis* (*Mb*) to simulate outbreak trajectories. Given the intractability of these model's
22 likelihood functions, we employ approximate bayesian computation, a numerical approach to assess
23 model distinguishability and identifiability across diverse outbreak scenarios representing several
24 initial risk compositions. By selecting the model that best fits early symptomatic dynamics, we infer
25 the most likely causative infectious agent and make informed individual antibiotic administration
26 decisions. Furthermore, we integrate an economic model to assess expected benefits of different
27 antibiotic treatment strategies. Results demonstrate a strong early infectious agent identification
28 performance with an average accuracy of 93%. Findings also highlight that pathogen-informed
29 treatment decisions substantially and consistently decreases antimicrobial usage (44%) across batch
30 configurations, contributing against the emergence of antimicrobial resistance. Informed-decisions
31 strategies also led to an overall moderate increase in net profit of 1%. This work, paves the way for
32 developing user-centered decision-support tools for BRD control.

33

34 **Keywords:** BRD pathogen inference, non-local numerical model distinguishability,
35 decision-informed control measures, Bioeconomic impact of informed-decisions,
36 computational epidemiology, decision intelligence

40 **1. Introduction**

41 Bovine Respiratory Disease (BRD) is one of the most significant health and economic challenges
 42 in the cattle industry, representing a substantial burden globally (Babcock et al., 2009; Delabouglise
 43 et al., 2017). Its economic impact is profound, with costs estimated to reach 20% of farmers' income
 44 in France and up to 44% in North America (Bareille et al., 2009; Mijar et al., 2023). BRD is a highly
 45 infectious, multifactorial disease affecting both the upper and lower respiratory tracts. It is
 46 commonly caused by co-infections of viruses and bacteria and is often exacerbated by abiotic
 47 stressors such as transportation stress (Grissett et al., 2015; Kudirkiene et al., 2021). In Europe, the
 48 most frequently reported pathogens include bacterial agents such as *Mycoplasmopsis bovis* (Mb)
 49 and *Mannheimia haemolytica* (Mh), alongside viral agents like Orthopneumovirus bovis(BRSV)
 50 and Respirovirus bovis (PI3) (Grissett et al., 2015). Diagnosing BRD is challenging due to the
 51 interplay of multiple factors, such as the nature of pathogens, animal genetics, and farming
 52 management practices (Gaudino et al., 2022; Murray et al., 2017). There is no global common
 53 threshold to determine whether an animal is diseased from clinical signs (fever, nasal discharge...)
 54 because clinical signs are non-specific to BRD, making precise pathogen identification difficult
 55 (Wolferger et al., 2015). Moreover, visual detection often results in delayed diagnoses. For instance,
 56 there can be a lag of up to 51 hours between the onset of hyperthermia episodes caused by the
 57 disease and observable clinical signs (Timsit et al., 2011). Laboratory tests such as multiplex PCR,
 58 while more accurate, are costly (up to \$150 per sample) and time-consuming, taking days to yield
 59 results (Thonur et al., 2012). Due to these diagnostic challenges, usually during an outbreak,
 60 causative pathogens are not precisely identified by farmers (Griffin et al., 2014; Ollivet et al., 2020).
 61 Antibiotics remain the primary control measure (Ollivett et al., 2020; Brault et al., 2019; Nickell &
 62 White, 2010), with farmers relying on visual signs of severe illness for treatment decisions (Ives et
 63 al., 2015). However, this empirical approach often leads to overuse and misuse of antibiotics,
 64 highlighting the problem of antimicrobial resistance and raising concerns for public health
 65 (consumers), animal welfare, and environmental management.

66 As modelling gains prevalence among policy makers in animal health (Sébastien Picault et al., 2024;
 67 Pauline Ezanno et al., 2022) or plant disease (Véronique Bellon-Maurel et al., 2022; Samuel Soubeyrand
 68 et al., 2024), modelling approaches have been increasingly viewed as a way to ensure that optimal
 69 decisions are taken based on evidence-based information. Modelling has become a tool for
 70 quantifying disease transmission, predicting outbreaks, and optimizing intervention strategies.
 71 Mathematical models provide a rigorous framework for integrating biological, environmental, and
 72 management factors, facilitating evidence-based decision-making (N. Cunniffe et al., 2020). In fact,
 73 some articles strongly argue that mathematical modelling is the best method for studying and
 74 understanding the spread of BRD (Pauline Ezanno et al., 2020), they allow interdisciplinary
 75 collaboration (inputs from epidemiologists, veterinarians, farmers...), they provide a framework to
 76 describe the multiscale interactions between hosts, pathogens and the environment; they allow the
 77 simulation of various scenarios such as the impact of control measures making them indispensable
 78 for proactive disease management. Numerous mechanistic models of BRD have been proposed to
 79 investigate the spread of BRD and the factors that impact the dynamics and transmission of its
 80 infectious pathogens (Baptiste Sorin et al., 2023; Sébastien Picault et al., 2022). Due to the high
 81 complexity implied in the mechanism of BRD spread, commonly used mathematical models for
 82 BRD vary widely in their level of detail and model structure. In addition to the difference in
 83 pathogen transmission mechanisms, co-infection mechanisms and detection from clinical signs
 84 mechanisms are not yet completely understood, therefore models are still being researched and build

85 with different assumptions. Comparative modelling is a way to ensure that forecasting efforts and
86 the evaluation of intervention strategies are conserved across the range of realistic model structures
87 (R. Meza et al., 2014; Elizabeth C. Lee et al., 2018). Three related concepts are useful to consider
88 in these efforts – First, model identifiability, addresses whether the parameters of a given model can
89 be uniquely estimated from available data which is critical, particularly for models having multiple
90 parameters and an intractable likelihood. Second, model distinguishability which is closely related
91 to model identifiability addresses whether competing models can be differentiated based on their
92 ability to fit empirical data (E. Walter et al., 1984) here the challenge lies in ensuring that models,
93 while potentially similar in structure, produce sufficiently distinct predictions or outcomes. Finally,
94 Decision impact assessment, addresses the practical consequences of model-based
95 recommendations. Beyond theoretical model distinguishability, it is essential to evaluate whether a
96 selected model leads to actionable and economically viable control strategies. A well-identified
97 model should not only reproduce observed outbreaks but also yield measurable benefits – such as
98 reduced antibiotic use, improved animal welfare, and increased farm profitability. This aligns with
99 recent advances in computational epidemiology, which emphasize the integration of decision-
100 theoretic principles in model selection (stevens et al., 2023).

101 In this study, we examine the effects of model structural differences on symptomatic outbreak
102 dynamics, considering three pathogen-specific BRD mechanistic models. Our goal is to determine
103 which model best explains a theoretically observed outbreak and, in doing so, identify the infectious
104 agent responsible for the disease. We then assess the practical relevance of this identification by
105 computing the expected economic impact of pathogen-informed interventions, quantifying the
106 average benefits of targeted antibiotic treatments based on model predictions. The selected models,
107 among the most recent and realistic in the literature, share a common individual-based, discrete-
108 time, and stochastic framework, originally developed to assess the influence of batch formation
109 policies on BRD transmission. Given their intractable likelihoods, we rely on numerical exploration
110 rather than explicit structural inference, allowing us to evaluate both distinguishability and
111 identifiability while systematically investigating all plausible epidemiological scenarios based on
112 individual risk-levels. This work is conducted from a theoretical perspective to validate the proposed
113 methodology, ensuring its robustness before potential application in real-world settings.

114 By integrating epidemiological modelling with economic assessment, this study not only advances
115 methodological approaches for pathogen inference but also provides a quantitative framework for
116 evaluating the financial trade-offs of model-driven decision-making. This work contributes to the
117 broader discourse on model selection in epidemiological modelling, offering a methodology that
118 balances modelling rigor, epidemiological relevance, and bio-economic feasibility.

119

120

121

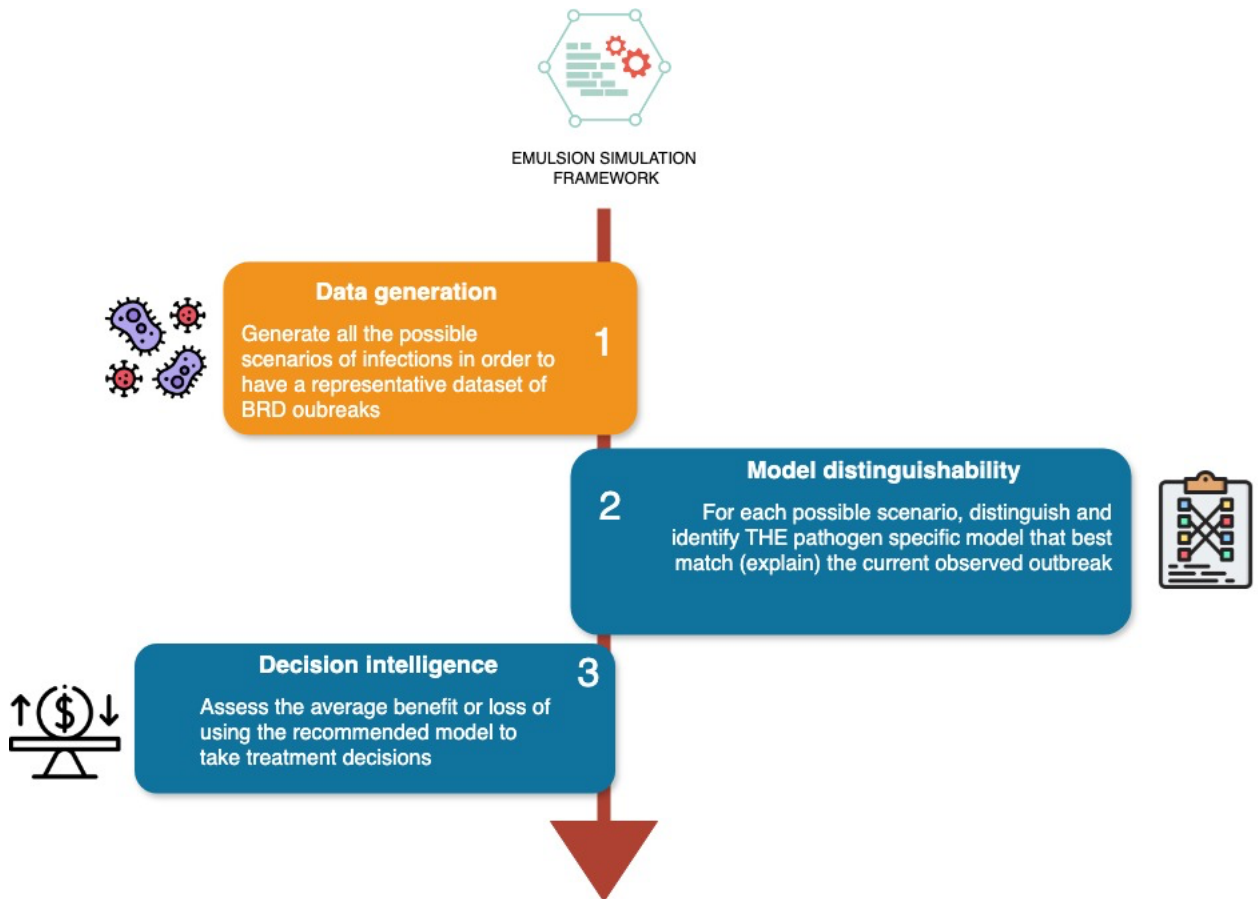
122 **2. Materials and methods**

123 **2.1. Overview of the methodological approach**

124 In this study, the three mechanistic models for BRD we focused on were originally developed and
125 published by (Sorin et al., 2023) and are described in section 2.2. Each model is tailored to one

126 of the most predominant pathogens: Orthopneumovirus bovis(BRSV), *Mannheimia*
127 *haemolytica* (Mh), *Mycoplasmopsis bovis* (Mb).

128



129

130 **Figure 1: Overview of the methodological approach.** The figure emphasizes a closed-loop
131 approach: generate diverse outbreak scenarios, identify the best explanatory pathogen model,
132 confirm that model's parameters can reliably be inferred, and finally evaluate the
133 bioeconomic or operational impact of using these model-based insights in real-world
134 settings.

135

136 EMULSION (Picault et al., 2019b) is a simulation framework designed to address the limitations
137 of traditional epidemiological models by enhancing flexibility and transparency in modelling complex
138 systems. It enables easier collaboration among different experts such as veterinarians, modeller,
139 farmers. Integrated with a versatile agent-based simulation engine, processes are represented using
140 finite state machines, allowing for detailed modelling of transitions, conditions, and actions. This
141 approach facilitates interdisciplinary collaboration and adaptability.

142 In the first step (Fig. 1 – box 1), we repurposed those pathogen-specific mechanistic BRD models
143 within the Emulsion simulation framework to construct synthetic time series of outbreak dynamics.
144 Specifically, we considered three batches of $N = 12$ animals each, observed over a limited period
145 of $T = 277$ days. Let $t \in \{0, 0.5, 1, \dots, 2T\}$ (measured in days) denote discrete 12-hour timesteps,

reflecting the average frequency at which farmers typically visually assess cattle for clinical symptoms (Sébastien Picault et al., 2022). For each pathogen-specific model, key parameters $\boldsymbol{\theta}$ were systematically varied within biologically plausible ranges. For a given parameter set $\boldsymbol{\theta}_k$, we numerically solved the underlying system of equations to obtain the number of symptomatic animals at each timestep, yielding a trajectory $\{y_t^{(k)} : t = 0, 0.5, 1, \dots, 2T\}$. By aggregating these simulations over all parameter configurations $k = 1, \dots, K$, we gathered a comprehensive synthetic dataset that closely mirrors conditions in French fattening operations and captures all the plausible BRD outbreaks based on individual risk-levels. Note that these models (see section 2.2) are stochastic and incorporate random effects of the detection method (visual assessment of clinical symptoms) ensuring that inherent randomness of biological systems are conserved.

In the second step (Fig. 1 – box 2), we focused on distinguishing three pathogen-specific models – each corresponding to a different BRD pathogen – based on a limited window of synthetic outbreak data (we assessed our methodology on the initial 5 days of simulated disease). Formally, if $\{y_t\}_{t=1}^{T^*}$ denotes the synthetic time series of symptomatic animals over the first $T^* = 5$ days, we computed a goodness-of-fit measure $\mathcal{L}(\mathcal{M}_i | \{y_t\}_{t=1}^{T^*})$ for each model \mathcal{M}_i , $i \in \{\text{Brsv, Mh, Mb}\}$. By comparing the good of fit between simulated outbreak and a reference trajectory designated as “true”, we identify which pathogen-specific model best explained the early-stage outbreak dynamics. Consequently, under certain assumptions (detailed in the Discussion section), if a farmer were to record the same 5 days of observations in a real-world scenario, they could analogously select the most likely pathogen responsible for the observed clinical signs, thereby enabling more targeted control and treatment strategies.

In the third and last step (Fig. 1 – box 3), we employed the “recommended” model, calibrated using the default parameters values from the original study (Baptiste Sorin-Dupont et al., 2023), which represent the average effects of each pathogen group. This model was then used to guide disease-control decisions over the remaining 273 days. Specifically, we computed the expected profit or loss, $\mathbb{E}[\text{Profit} | \mathcal{M}_{\text{recommended}}]$, to quantitatively, assess the potential benefits of a pathogen-informed treatment decision system, including its impact on antimicrobial usage and the net profit.

173

174 2.2. Model descriptions

175 The most realistic mechanistic models are stochastic models, designed to evaluate how batch
176 composition and size influence pathogen spread and intervention outcomes (Baptiste Sorin-Dupont et
177 al., 2023). These individual-based stochastic models integrate viral and bacterial pathogens and
178 account for individual risk levels, providing insights into disease dynamics and control strategies. In
179 the paper, we employed the latter models because they are representative of the different pathogen
180 effects on the spread of BRD, ranging from acute outbreaks (BRD) to opportunistic bacterial
181 infections (*Mh*) and chronic persistence (*MB*)

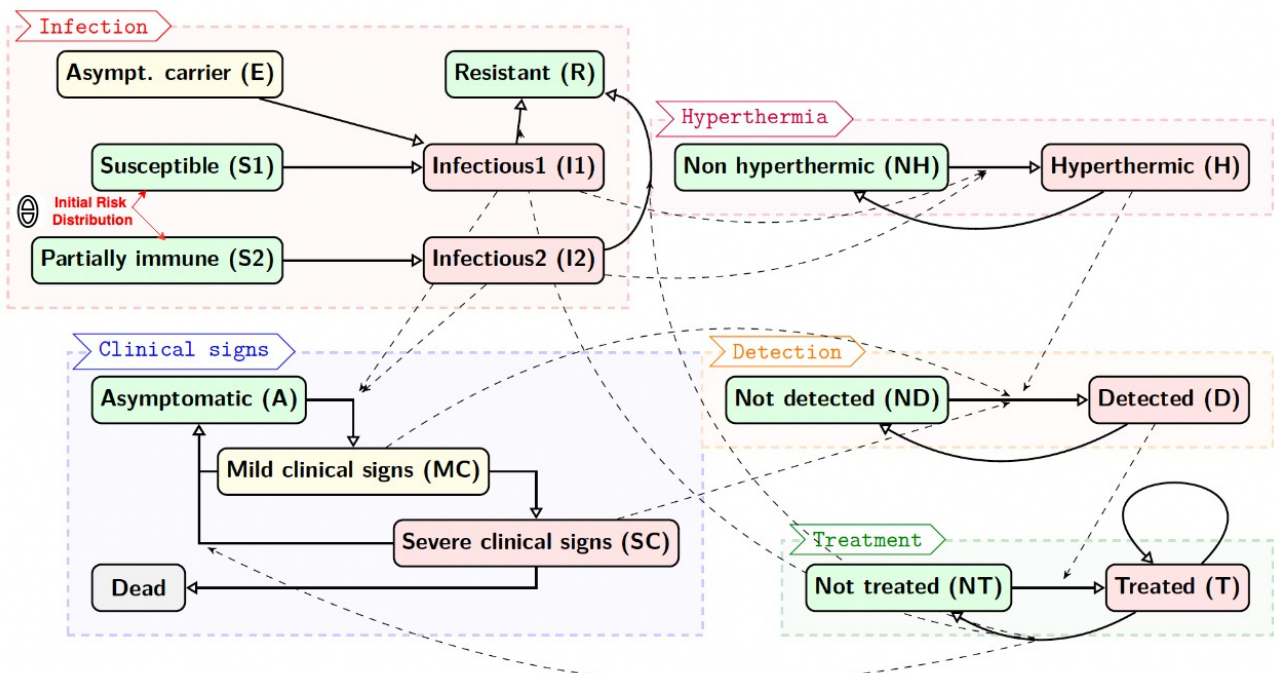
182

183 2.2.1. Orthopneumovirus bovis(BRSV) infection model

184 This model describes the transmission of BRSV (Kurucay H.N. et al., 2025), a highly contagious

185 airborne virus with rapid spread dynamics. It follows a stochastic compartmental structure, where
 186 individuals can begin as susceptible (S1, S2) and can be infected either for the first time (I1) or as
 187 reinfections (I2), with reinfected individuals exhibiting reduced infectiousness. Individuals can
 188 become asymptomatic carriers (E) before progressing to an infectious state. After infection,
 189 individuals eventually recover and transition to the resistant (R) state. Clinical states include mild
 190 clinical signs (MC), which may escalate to severe clinical signs (SC), with a probability of
 191 developing severe illness. Severe cases have a risk of mortality, leading to a transition to the dead
 192 state if the disease is too severe. Detection of diseased animals relies on clinical symptoms, with
 193 severe cases more likely to be detected. Detection leads to treatment (T), which may succeed,
 194 causing individuals to transition back to asymptomatic (A), or fail, requiring multiple rounds of
 195 treatment. Hyperthermia (H) also plays a role in detection, as infected individuals may exhibit fever,
 196 increasing their likelihood of being diagnosed. A key feature of this model is the incorporation of
 197 partial immunity.

198



199

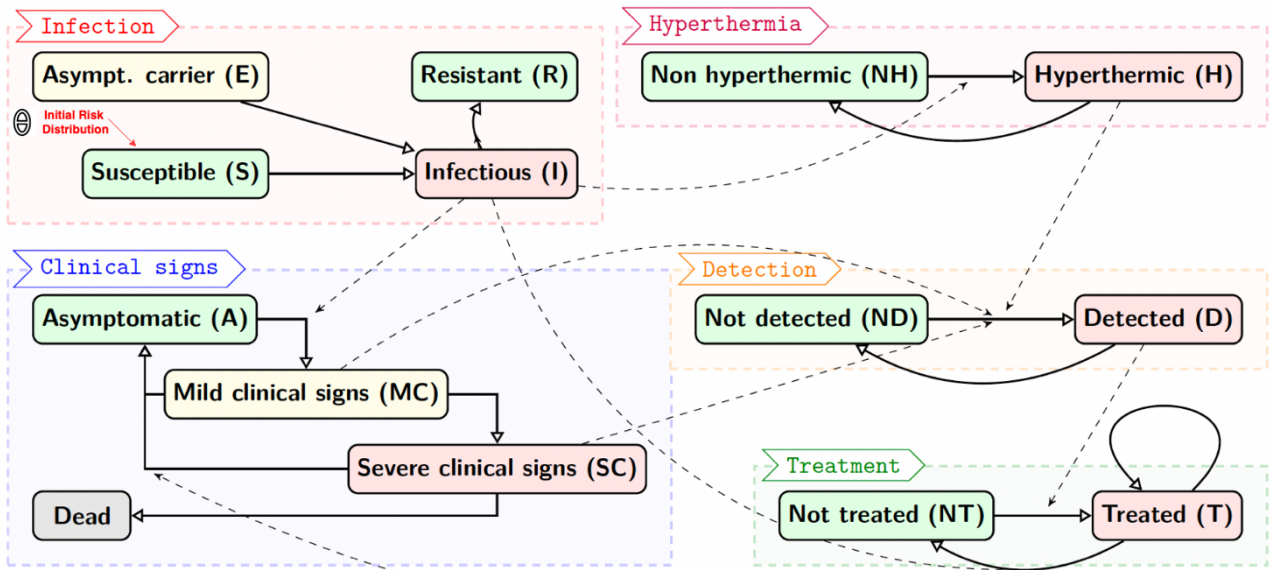
200 **Figure 2: Model overview for BRSV.** The model incorporates four processes (infection,
 201 clinical signs, hyperthermia, detection, treatment) associated to individual states (rounded
 202 boxes), which could evolve themselves (plain arrows) but also influenced each other (dashed
 203 arrows). Figure adapted from (Baptiste Sorin-Dupont et al., 2023).

204

205 2.2.2. *Mannheimia haemolytica* (Mh) infection model

206 This model represents the transmission of *Mh* (Mohamed R.A et al., 2008), a bacterial pathogen
 207 with opportunistic behaviour, often colonizing the respiratory tract before causing disease under
 208 stress-induced immunosuppression. The model includes susceptible (S) individuals who may

209 transition into asymptomatic carriers I before becoming infectious (I). unlike BRSV, there is no
 210 reinfection state, as infection leads to either clearance or severe disease. The progression of clinical
 211 signs follows the same patterns as for the BRSV model. Severe cases may either recover, die, or
 212 be detected and treated (T). Detection of diseased animals occurs through clinical observation and
 213 hyperthermia (H), which increased detection probability. Treatment is also modelled in the same
 214 way as for BRSV model.



215
 216 **Figure 3: Model overview for *Mh* & *Mb*.** The model incorporates four processes (infection,
 217 clinical signs, hyperthermia, detection, treatment) associated to individual states (rounded
 218 boxes), which could evolve themselves (plain arrows) but also influenced each other (dashed
 219 arrows). Figure adapted from (Baptiste Sorin-Dupont et al., 2023).

220 221 2.2.3. *Mycoplasmosis bovis* (*Mb*) infection model

222 The third and last model (*Mb*) incorporated chronic infection dynamics, characterized by a slow-
 223 spreading, long-term colonizing bacterial pathogen causing intermittent clinical signs (Bürki S. et
 224 al., 2015). The states machines describing the infection mechanisms of *Mb* (Infection, clinical signs,
 225 hyperthermia, detection, treatment) are identical to those of *Mh*. However, unlike *M. haemolytica*,
 226 nominal values of the parameters of *M. bovis* are such the model expresses long-term persistence,
 227 with some infectious individuals (I) failing to recover fully, remaining chronic carriers. Detection
 228 is particularly challenging, as *Mb* infections can be subclinical for extended periods (Maunsell F.P.
 229 et al., 2009), making early diagnosis unreliable. In this model, infection durations are prolonged.
 230 The model is well-suited for studying persistent infections. The structure of this model is identical
 231 to that of *Mh* and is represented in figure 3.

234

2.3. Generating BRD outbreak scenarios

235

2.3.1. Models' baseline parameters

236

Each epidemiological simulation starts with a predefined initial condition, which specifies the composition of the batch in terms of individual risk levels. Let $\theta = (\theta_L, \theta_M, \theta_H)$ (Fig. 2 & 3) with the constraints $\theta_L, \theta_M, \theta_H \in [0, 1]$ such that $\theta_L + \theta_M + \theta_H = 1$. Where θ is a vector representing the proportion of individuals in each risk category and $\theta_L, \theta_M, \text{and } \theta_H$ denote the fractions of low, medium, and high-risk individuals in the population respectively. These proportions are essential for defining the starting point of the simulations, as they determine the susceptibility and transmission potential within a group. The effects of θ are pathogen-dependent. Highly contagious viruses such as BRSV exhibit rapid spread dynamics, whereas opportunistic bacterial infections like *Mh* are more influenced by host immunity and stress-related susceptibility. Chronic pathogens such as *Mb* could depend heavily on θ_H , as the persistence of infected individuals in the population prolongs transmission and sustains pathogen circulation. The structure of θ thus dictates outbreak intensity, disease persistence, and the effectiveness of control interventions, making it a crucial parameters vector in the modelling of BRD dynamics. While these parameters are the most important, they are common across all models. Additional information on specialized parameters for each model can be found in the original paper published (Baptiste Sorin et al., 2023).

252

253

2.3.2. Reference synthetic outbreak scenario generation

254

To mimic the average settings in real fattening farms in France, we considered 1 batch composed of 12 animals. Given that risk levels are discrete and partitioned into three categories, for N=12, the number of batch composition follows a combinatorial constraint and results in a total of 91 distinct settings. The number of valid allocations can be derived using the stars and bars theorem, where N identical objects (animals) are distributed into $k = 3$ and S serves as the space of initial conditions for the simulations. Increasing N (the total number of animals) would expand the space S exponentially, making simulations computationally more demanding. Each $\theta \in S$ was used as an initial condition for each of the three pathogen-specific mechanistic models $\mathcal{M}_i = \{\text{Brsv}, \text{Mb}, \text{Mb}\}$, however since these models are stochastic, running the same model on the same parameters will yield slightly different results. To capture this variability that is also present in the real-world, we made sets of repetition ($r = 50$) for each combination of $\theta \in S$: $\mathcal{M}_i(\theta_j)^{(k)}$ with $k = 1, \dots, r$. Each repetition is then used as input for the mechanistic models. Thus, for each (θ, \mathcal{M}) pair, we conduct r independent runs. The choice of $r = 5$ repetitions is a reasonable trade-off that balances computations efficiency and results stability. Each simulation produced a trajectory over time for each state variable defined in the model description section, including the observed symptomatic individuals. Thus, the final dataset consisted of: $|S| \times |\mathcal{M}| \times r = 91 \times 3 \times 50 = 13650$ simulated realistic BRD outbreaks, 150 cases (3 pathogens \times 50 repetitions) for each of the 91 initial conditions. All model simulations and computations were done using Python 3.8 and using Emulsion simulation engine (Version 1.2rc6).

273

Algorithm 1 Simulation Design for Synthetic Dataset

```
1: Define experimental setup:
2: Set batch size  $N = 12$ .
3: Compute the set  $\mathcal{S}$  of valid risk allocations using the combinatorial formula.
4: Define the set of mechanistic models  $\mathcal{M} = \{M_{\text{BRSV}}, M_{\text{MH}}, M_{\text{MB}}\}$ .
5: Set the number of repetitions  $r = 50$ .
6: for each initial risk composition  $\boldsymbol{\theta}_j \in \mathcal{S}$  do
7:   for each pathogen model  $M_i \in \mathcal{M}$  do
8:     for each repetition  $k = 1, \dots, r$  do
9:       Initialize empty set  $\mathcal{O}$  for storing stochastic outputs.
10:      Simulate model  $M_i(\boldsymbol{\theta}_j)^{(k)}$  to obtain trajectory  $O_k$ .
11:      Store  $O_k$  in  $\mathcal{O}$ .
12:    end for
13:  end for
14: end for
15: Finalize dataset:
16: Aggregate all trajectories into structured dataset.
17: The final dataset contains  $|\mathcal{S}| \times |\mathcal{M}| \times r$  simulations.
```

274
275
276
277
278
279

Algorithm 1: Simulation setup for synthetic data generation. A batch of 12 young calves was partitioned into 91 possible combinations of initial risk levels. Each combination was fed with repetition into 3 pathogen-specific mechanistic models, with 50 stochastic & independent runs per model. In total, 13 650 simulation points were generated to generate biophysical-driven dynamics.

280
281
282

2.4. Inverse modelling – Distinguishing & recognizing BRD infectious agents from observations

283 Model distinguishability refers to differentiating between competing models in a theoretical setting,
284 as opposed to model selection, which applies when working with real-world data. Since we do not
285 analyse the analytical form of these models but instead solve them numerically, our approach falls
286 under numerical distinguishability. This distinction is crucial, as it allows us to systematically assess
287 key hypotheses and evaluate the theoretical structure of these models without the logistical
288 constraints of setting up a full-scale experimental study with veterinary observations. Given an
289 observed outbreak S^* , the objective of model distinguishability is to identify the model \mathcal{M}_i that
290 best explains the observations: $\hat{M} = \arg \max_{M_i \in \mathcal{M}} P(M_i | S^*)$. Where $P(M_i | S^*)$ represents the posterior
291 probability of model \mathcal{M}_i given the observed summary statistics S^* . However, the likelihood function
292 $P(M_i | S^*)$ is intractable for the BRD models under consideration partly due to their stochastic nature
293 and high-dimensional latent space. Consequently, we relied on likelihood-free inference methods,
294 notably the Approximate Bayesian Computation (ABC) (Beaumont et al., 2019), that bypasses
295 explicitly likelihood evaluation.

296 Instead of directly computing the likelihood $P(\mathbf{S}^*|\theta)$, ABC relies on simulating data under different
 297 parameter values and comparing the resulting summary statistics with the observed data. The key
 298 idea is to sample parameters θ from a prior distribution, generate synthetic data using a mechanistic
 299 model, and compute a distance metric between simulated summary statistics \mathbf{S} and observed
 300 summary statistics \mathbf{S}^* . Parameter values yielding summary statistics within a predefined tolerance
 301 ε are retained, forming an approximation of the posterior distribution $P(\theta|\mathbf{S}^*)$.

302 Approximate Bayesian Computation also enables model distinguishability when the likelihood
 303 function is intractable. We use model indicator $i = \{ \text{BRSV}, Mh, Mb \}$ which represent the set of
 304 candidate models $\mathcal{M} \in \{\text{BRSV}, Mh, Mb\}$. We sample $i \sim \pi(I)$ from the prior distribution over
 305 models and treat it as a categorical variable in the ABC framework. After generating simulated
 306 summary statistics (vector composed of symptomatic dynamics) for each model, we apply
 307 multinomial logistic regression to estimate the posterior probability $P(I = i|\mathbf{S} = \mathbf{S}^*)$ (Fagundes et
 308 al., 2007). We make the regression estimate locally around \mathbf{S}^* in the same way as in the standard
 309 ABC approach using the same summary statistics as in (Eyango et al., 2024), specifically only the
 310 top 10% simulations closest to the observations are retained, and these are weighted by a gaussian
 311 kernel.

312 Every single outbreak from the 1365 realistic BRD outbreaks simulated in the previous section (cf.
 313 *Reference synthetic outbreak scenario*) was regarded as the true observations in the ABC framework
 314 and model distinguishability was performed on them. Our dataset consists of systematically varied
 315 initial conditions per model with 50 repetitions per condition, it provides a uniform representation
 316 of all possible discrete outbreak initial compositions.

Algorithm 2 Distinguishing BRD pathogen-specific mechanistic models

- 1: **Input:** Set of observed outbreaks S^* , candidate models \mathcal{M} , prior distributions $\pi(\theta)$, repetitions r
- 2: **Output:** Inferred model $\hat{\mathcal{M}}$, classification accuracy \mathcal{A} , and performance metrics
- 3: **for** each observed outbreak S_j^* **do**
- 4: **for** each candidate model \mathcal{M}_i **do**
- 5: **for** each repetition $k = 1, \dots, r$ **do**
- 6: Sample parameters $\theta_i^{(k)} \sim \pi(\theta)$
- 7: Simulate summary statistics $\mathbf{S}_i^{(k)}$ from $\mathcal{M}_i(\theta_i^{(k)})$
- 8: Retain top 10% closest $\mathbf{S}_i^{(k)}$ to \mathbf{S}_j^* using distance metric $d(\mathbf{S}, \mathbf{S}^*)$
- 9: Apply Epanechnikov kernel weighting to retained simulations
- 10: Perform multinomial logistic regression to estimate $P(\mathcal{M}_i|\mathbf{S}_j^*)$
- 11: Get $\hat{\mathcal{M}}_j = \arg \max_i P(\mathcal{M}_i|\mathbf{S}_j^*)$
- 12: Compute overall classification accuracy:

$$D_j = \frac{1}{r} \sum_{k=1}^r \mathbf{1}(\hat{\mathcal{M}}_j^{(k)} = M_j)$$

- 13: Compute additional performance metrics: Sensitivity ...
- 14: **end for**
- 15: **end for**
- 16: **end for**

318
 319 **Algorithm 2:** model distinguishability using Approximate Bayesian Computation with
 320 multinomial logistic regression. This process outputs the inferred pathogen-model and the
 321 performance metrics, such as the accuracy.

321 This distinguishability index (accuracy) measures the proportion of cases where the selected model
 322 matches the true model and varies in the range [0,1], higher values indicate better distinguishability
 323 among models. To get even further, since model distinguishability is inherently a classification
 324 problem, we further evaluate performance using standard classification metrics, particularly:

325 Table 1: Distinguishability performance metrics

Metrics	Formula	Description
True Positive Rate (Sensitivity or Recall)	$TPR_{M_i} = \frac{TP_{M_i}}{TP_{M_i} + FN_{M_i}}$	Probability of correctly identifying the true pathogen. Important for ensuring correct treatment when the pathogen is actually present
False Positive Rate (1 – Specificity)	$FPR_{M_i} = \frac{FP_{M_i}}{FP_{M_i} + TN_{M_i}}$	Probability of wrongly assigning a pathogen when it is not present. Important for estimating the cost of inadequate control measures
Positive Predictive Value (Precision)	$PPV_{M_i} = \frac{TP_{M_i}}{TP_{M_i} + FP_{M_i}}$	Probability that a predicted pathogen is actually the correct one. Useful for guiding confidence in the decision
Negative Predictive Value	$NPV_{M_i} = \frac{TN_{M_i}}{TN_{M_i} + FN_{M_i}}$	Probability that a rejected pathogen is actually absent. Important for minimizing unnecessary treatments.

326 The full distinguishability procedure was conducted in R programming language, using the ABC
 327 package (version 2.2.2; [Csilléry et al., 2012](#)).

328

329 2.5. Bioeconomic impact - Expected profit/loss of pathogen-informed treatments

330 2.5.1. A simple economical model

331 The economic model used in this study was inspired by a veterinary thesis ([Théo Salles, 2024](#)) on a
 332 mechanistic model of BRD and by insights from an “Inosys Réseaux Elevage” report ([Benoteau G.
 333 et al., 2023](#)). In particular, Inosys’ case type methodology, which reconstructs representative farm
 334 systems through collective modelling and field expertise.

335 The economic model developed evaluates the net profit at the end of the fattening period by
 336 calculating the difference between total revenues generated from cattle sales and the direct costs
 337 incurred during the fattening process. This approach is a simplified version, which excludes indirect
 338 costs, focusing solely on tangible, easily measurable expenditures and earnings directly linked to
 339 animal health and fattening performance. The net profit (Δ) is defined as: $\Delta = R - C$ (1). Where R
 340 represents the total revenues from cattle sales and C denotes the total costs. Total revenues R are
 341 calculated based on the sale of fattened cattle, taking into account the carcass weight and conformation
 342 grade influenced by the health status during the fattening period and costs C include purchase costs

343 of calves, feed costs, medical treatment costs, and veterinary services' costs.

344 The purchase costs are computed as: $C_{purchase} = N_{calf} \cdot P_{calf}$ (2). Where N_{calf} is the total number
345 of calves purchased by the farmer, and P_{calf} is the price per calf. The purchase price of a calf in is
346 1185€, it is the average price used in typical Charolais fattener farms in Brittany published by "Inosys
347 réseaux d'élevage" (Benoteay G. et al., 2023).

348 The feed costs primarily represent the feeding expenses of animals, calculated as: $C_{production} =$
349 $F_{cost} \cdot \sum WG_{status}$ (3). Where WG_{status} is the cumulative weight gain (depending on the clinical
350 status \in asymptomatic, mild, severe) of all the animals by the end of fattening period, and F_{cost}
351 represents the feed cost per kilogram, set at €0.9 per kg of live weight. The cumulative weight gain is
352 a function of daily weight gain (GMQ) and the durations of the fattening period (D), expressed as:
353 $WG_{status} = GMQ_{status} \cdot D$. The average fattening period (D) in France is estimated at 277 days (Théo
354 Salles, 2024). The GMQ values vary depending on the animal's health status: 1.388 kg/day for
355 asymptomatic, 1.080 kg/day for mild cases, and 0.925 kg/day for severe cases (Benoteau G. et al.,
356 2023). For healthy animals. The decline in GMQ was calculated by Blakebrough-Hall (Blakebrough-
357 Hall C et al., 2020) on Charolais et also by Théo Salles (Théo Salles, 2024)

358 Treatment costs are determined by the number of individual treatments administered (antibiotics) and
359 the cost per treatment: $C_{treatment} = N_{doses} \cdot P_{treatment}$ (4). Where N_{doses} is the total number of
360 antibiotic doses administered by the end of fattening period, and $P_{treatment}$ is the unitary price of
361 antibiotics set at an average of €13 (Théo Salles, 2024).

362 The cost of veterinarian services is calculated based on the time taken to administer individual
363 antibiotic and the hourly price of veterinary services: $C_{veterinary} = N_{doses} \cdot t_{treatment} \cdot P_{veterinary}$
364 (5). Where N_{doses} is the total number of antibiotic doses administered by the end of fattening period,
365 $t_{treatment}$ is the average time spent to perform an individual antibiotic treatment estimated at 40 min
366 (0.67 hours) (Wang et al., théo salles, 2024), $P_{veterinary}$ is the hourly veterinary price estimated at
367 €9.94 in France from the Convention Collective Nationale Agricole (CCNA).

368 Revenue from cattle sales is influenced by the carcass weight and conformation grade by the end of
369 the fattening period which are dependent on the animal's health status during fattening. The total
370 carcass weight is computed as: $CW_{status} = N_{status}^{alive} \cdot (W^0 + WG_{status}) \cdot CY$. Where N_{status}^{alive} is the
371 number of alive cases per clinical status. Note that for individuals that died during the fattening period,
372 their buying and feed costs and kept (they increase the costs), however for the selling, they were
373 subtracted. W^0 is the initial weight of an animal and WG_{status} is the weight gained (depending on
374 the clinical status) by an animal by the end of fattening period as defined above and CY is the carcass
375 yield (estimated at 0.58) that allows to convert live weight into carcass weight for young beef
376 Charolais (Lefrand I et al., 2019). That formulation supposes that all the calves are bought with the
377 same weights. The conformation quality (Table 2) refers to the muscle development and shape of an
378 animal's carcass, which affects its market prices and is graded from high (U) to lower (R) (Duflot B.,
379 2023; These de Joly; Théo Salles, 2024).

380

381

382 Table 2. Impact of health status on carcass conformation and sale price

Conformation	Price	Proportions
--------------	-------	-------------

		Asymptomatic	Mild signs	Severe signs
R	5.25 €/kg	20%	60%	100%
U	5.41 €/kg	40%	40%	0%

383

384 The sales revenue is a weighted sum of these factors, reflecting the impact of health status on carcass
 385 quality and market price: $R_{sales} = CW_{status} \cdot (Prop_{status}^R \cdot (P_R - P_U) + P_U)$ (6). Where $Prop_{status}^R$
 386 is the proportion of conformation R (table xx) depending on their clinical status, P_R and P_U are the
 387 slaughter price of animals in conformation R and U.

388 Thus, the economic model (Δ) in Eq. (1) can be detailed as:

$$389 \Delta = N_{status} \cdot [W^0 + (GMQ_{status} \cdot D)] \cdot CY \cdot (Prop_{status}^R \cdot (P_R - P_U) + P_U) - N_{calf} \cdot P_{calf} - \\ 390 F_{cost} \cdot \sum(GMQ_{status} \cdot D) - N_{doses} \cdot (P_{treatment} - t_{treatment} \cdot P_{veterinary}) \quad (7)$$

391 Our simplified economic model operates under the assumption that weight loss due to disease is
 392 exclusively related to the time spent in diseased states (mild and severe). At the end of the fattening
 393 period, all the animals are sold at the same time: No special interventions are made to compensate for
 394 weight loss; feed costs and weight gain are considered linear, unaffected by other environmental or
 395 management factors. Our net profit is calculated only during the fattening period, and therefore is not
 396 the same as the net profit of the farm. The net profit we computed is related to beef bovine fattening
 397 and BRD control measures meanwhile the farm net profit is a larger notion that includes for instance,
 398 costs of energy, buildings, and government aid.

399

400 2.5.2. Integration with Mechanistic models

401 In this subsection, we describe the integration of mechanistic BRD models with our economic model.
 402 The mechanistic models simulate the progression of BRD at the individual animal level, generating
 403 outputs that reflect the dynamics (infection, clinical signs, detection, treatment) over time. These
 404 outputs are essential for translating biological processes into quantifiable economic impacts, such as
 405 weight gain, feed efficiency, and treatment costs. Default outputs are described in model description
 406 subsection (see 2.2), additional outputs required to run our economic model are described in table 3:
 407

408 Table 3: Table of Key variable linking mechanistic outputs to economic inputs

Mechanistic model output	Description	Impact
Asymptomatic count	Number of asymptomatic animals detected by the end of the fattening period	Healthy animals maintain higher daily weight gain, leading to increased sale weights and quality (conformity)
Mild count	Number of animals detected presenting mild clinical signs	Reduced feed efficiency increases costs while lowering final weight
Severe count	Number of animals detected presenting clinical signs	Severe cases drastically reduce weight gain and increase feed inefficiencies
Dead	Total number of dead animals	They increase the costs (buying, feed,

antibiotics), and decrease the sells (no revenue from them)

Treatment doses	Cumulative number of doses administered	-
Batch size	Number of animals per batch (batches have an equal number of individuals)	-
Batch number	Number of batches	-

409

410

411

412 *2.5.3. Estimating the expected profit/loss*

413 The objective of computing the expected profit or loss is to quantify the financial impact of decision
 414 errors in pathogen identification. To quantify the expected profit or loss resulting from model-informed decisions, we define a random variable Π representing the net profit (cf. 2.5.1) associated
 415 with pathogen identification outcomes. The decision-making process can lead to four possible
 416 outcomes: correctly identifying bacterial infections (B^+), incorrectly diagnosing a viral infection as
 417 bacterial (V^+), incorrectly diagnosing a bacterial infection as viral (B^-), and correctly identifying viral
 418 infections (V^-). Each of these outcomes influences both treatment decisions and their financial
 419 consequences. Let \mathcal{X} be a discrete random variable representing the outcome of pathogen
 420 identification, taking values in the set $\{B^+, B^-, V^+, V^-\}$. The probability mass function $P(\mathcal{X}=x_i)$
 421 corresponds to the proportion of each outcome in the confusion matrix. For instance, comparing
 422 bacteria to virus in our case (Table 4):
 423

424

425

Table 4: Confusion matrix. Illustrates the four possible outcomes for antibiotic treatment decisions

		Relevance of antimicrobial treatment	
		Needed	Not needed
Decision	treatment	Correctly identifying bacterial infections ($B^+ = \text{Correct recommendation}$)	Incorrectly identifying a viral infection as bacterial ($V^+ = \text{False alarm}$)
	no treatment	Incorrectly identifying a bacterial infection as viral ($B^- = \text{Missed opportunity}$)	Correctly identifying viral infections ($V^- = \text{Correct rejection}$)

426

427

428

429

430

431

432

433

434

The default decision rule is that any animal exhibiting clinical signs is systematically treated. This approach leads to two possible outcomes: either the animal is truly infected with a bacterium and receives antibiotic treatments (B^+), or it is infected with a virus yet receives antibiotic treatments (V^+). Without prior information about the true prevalence of pathogens, the expected net profit under this rule is calculated as the simple average of the net profits associated with these two outcomes:
 $E[\Delta]_{\text{default}} = \frac{1}{2} [\Pi(B^+) + \Pi(V^+)]$.
 In contrast, if the treatment is tailored to the pathogen type, the decision process distinguishes among four outcomes: B^+ , B^- , V^+ , V^- . The expected profit $E[\Delta]_{\text{informed}}$ is then calculated as:

435
$$E[\Delta]_{\text{informed}} = \sum_{x \in \{\text{B+}, \text{B-}, \text{V+}, \text{V-}\}} P(X = x) \cdot \Pi(x)$$

436
437 where $\Pi(x)$ denotes the net profit as computed in the previous part (2.5.1) associated with outcome
438 x . The probabilities of each event can be computed as: $P(X = x) = \frac{N_{X=x}}{N_\Omega}$ where $N_{X=x}$ is the count
439 of outcomes for event x and N_Ω is the total number of cases in the sample space Ω . Assuming that
440 the benefits of correct treatment and the cost savings from avoiding unnecessary treatments outweigh
441 the losses incurred from mis-identification.

442
443
444 *2.5.4. Case study: 5 days of observing before taking a treatment decision*

445 To illustrate the application of our methodology, we conducted a case study. Imagine a situation
446 where a BRD outbreak occurs in beef cattle farm managing one batch of 12 animals. At the onset
447 of the outbreak, the farmer has no prior information regarding the nature of the infectious agent.
448 The only observable metric for the farmer is the number of symptomatic animals detected daily.
449 However, due to non-specificity of clinical signs and the tendency of some animals to conceal
450 symptoms, the observed number of symptomatic cases is consistently lower than the actual number
451 of infected animals.

452 For five consecutive days, the farmer records the total number of symptomatic animals detected
453 each day. This limited dataset is then employed in our methodology to distinguish and infer the
454 most probable pathogen-model responsible for the outbreak. Based on the inferred pathogen, we
455 recommend specific control measures: If the pathogen is identified as bacterial, we advise treating
456 the detected symptomatic animals with antibiotics. And if the pathogen is viral, we recommend not
457 treating, as antibiotics would be ineffective.

458 The pathogen-specific model is subsequently used to forecast the progression of the disease for the
459 remainder of the fattening period. In France, the fattening period for beef cattle typically can last
460 until the animals reach up to 24 months of age ([Théo Salles, 2024](#)). This forecast provides insights
461 into the expected trajectory of the outbreak, including potential weight loss, treatment needs, and
462 overall animal health impacts.

463 We then integrated these forecasts into our economic model to estimate the expected profit or loss
464 under the recommended intervention strategy. This process allows us to assess the financial
465 implications of model-driven decision-making. Furthermore, this methodology was applied to all
466 the BRD outbreak scenarios generated (see [Section 2.3.2](#)). By evaluating the expected profit and
467 loss across diverse epidemiological conditions, it enable to comprehensively assess the profitability
468 and robustness of our pathogen identification method, ensuring its applicability and effectiveness
469 in real-world outbreak situations.

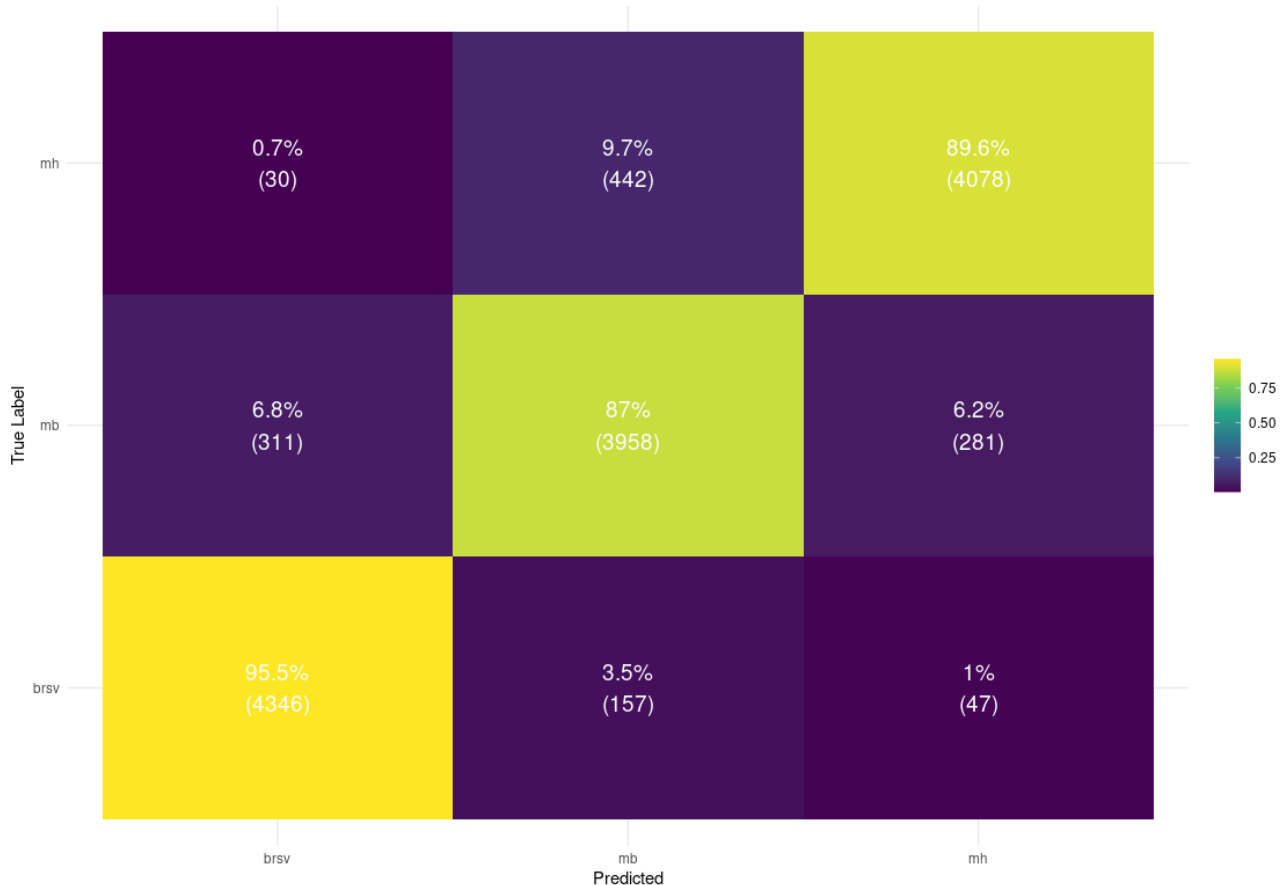
470

471 **3. Results**

472 *3.1. BRD Model distinguishability - a BRD infectious agent identification method*

473 *3.1.1. Performance assessment*

474



475
 476 Figure 4: Confusion matrix. Classification performance for BRSV, *Mh* and *Mb*. The
 477 diagonal represents correctly classified instances, while off-diagonal values indicate
 478 misclassifications between classes.

479
 480
 481
 482
 483 Table 5. Pathogens identification performances

Metrics	BRSV	<i>Mb</i>	<i>Mh</i>
True Positive Rate	0.96	0.87	0.90
False Positive Rate	0.04	0.07	0.04
Positive Predictive Value	0.93	0.87	0.93
Negative Predictive Value	0.98	0.93	0.95
Balanced Accuracy	0.96	0.90	0.93
Support	4550	4550	4550

484

485 We evaluated the capability of our methodology to distinguish among three BRD-causing
 486 pathogens, Orthopneumovirus bovis (BRSV), *Mannheimia haemolytica* (*Mh*), and *Mycoplasmopsis*
 487 *bovis* (*Mb*) using synthetic symptomatic trajectories recorded over the first five days of an outbreak.
 488 Our analysis is based on a confusion matrix (Figure 4) and key classification metrics presented in

489 **Table 5**, which include the true positive rate (TPR), positive predictive value (PPV), and false
 490 positive rate (FPR).

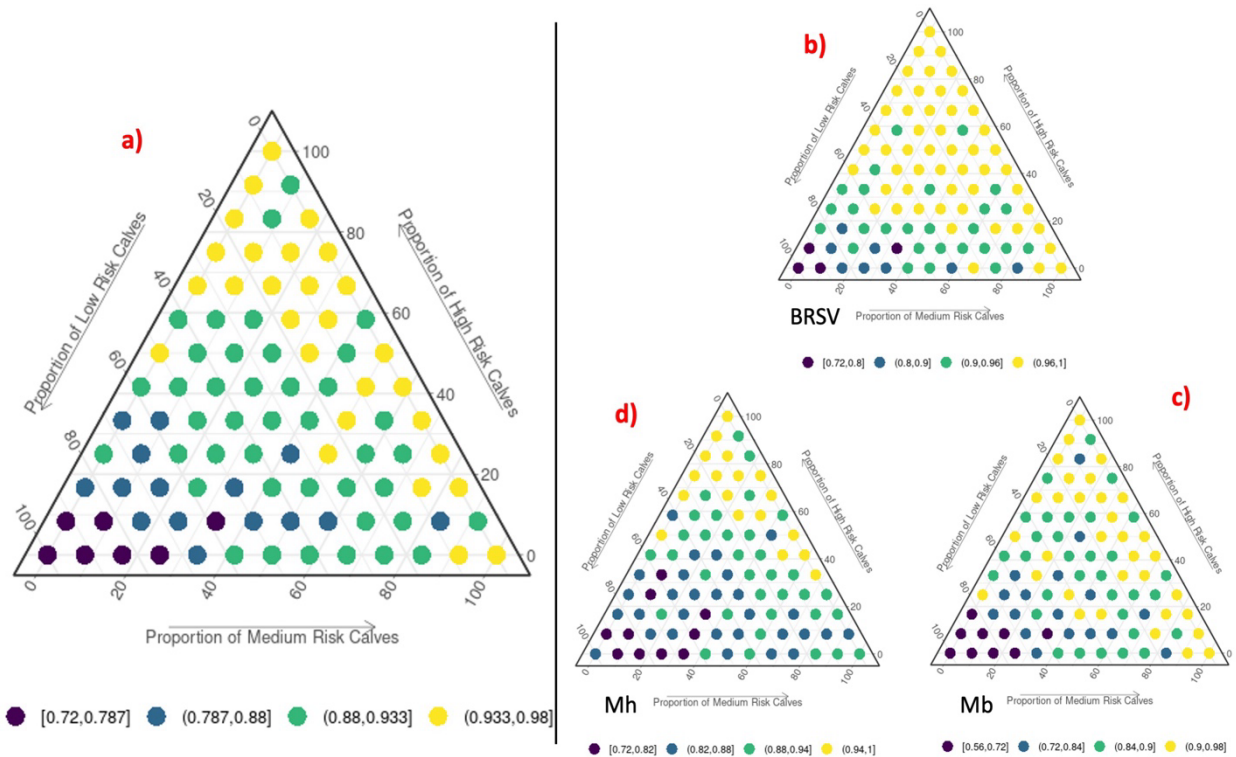
491 Distinguishing BRSV model amongst other models demonstrated the highest performance,
 492 achieving a TPR of 96% and a PPV of 93%, with an FPR of only 4%. These metrics indicate that
 493 the symptomatic progression associated with BRSV is distinct enough to allow for reliable
 494 identification, with minimal misclassification. When errors did occur, BRSV cases were primarily
 495 confused with Mb (3.5%), suggesting a minor overlap in their symptom profiles.

496 In contrast, the *Mh* model displayed a TPR of 90% and a PPV of 93%. However, about 9.7% of *Mh*
 497 cases were misclassified as Mb, which implies that the symptomatic trajectories of these bacterial
 498 infections share certain similarities that challenge precise differentiation. Mb itself was the most
 499 difficult to classify, with both a TPR and PPV of 87%. Misclassification for Mb was higher, with
 500 6.2% of cases being mistaken for *Mh* and 6.8% for BRSV, highlighting the subtle nature of its
 501 symptomatic signal.

502 Overall, the framework achieved robust classification performance for BRSV and *Mh*, while the
 503 identification of Mb presented additional challenges due to overlapping symptom dynamics.

504

505 3.1.2. Pathogen identification according to batch configurations



506

507 Fig 5: Pathogen distinguishability map after 5 days of observing of symptomatic dynamics. They
 508 represent the balanced accuracy of pathogen identification as a function of batch initial risk
 509 composition. The large ternary plot on the left is the overall classification accuracy. And on the right
 510 are the specific accuracies of each pathogen.

512 We next evaluated how the initial risk composition of a batch influences the accuracy of pathogen
 513 identification. [Figure 5.a](#) displays a ternary plot that maps balanced accuracy across varying
 514 proportions of low-, medium-, and high-risk individuals, revealing three distinct zones: high accuracy
 515 ($\geq 93\%$), moderate accuracy (88%–93%), and low accuracy (72%–78%). Batches dominated by high-
 516 risk individuals consistently achieved high accuracy, exceeding 93% in most cases. This suggests that
 517 the pronounced symptomatic trajectories in high-risk populations generate distinct outbreak
 518 dynamics, thereby facilitating more reliable pathogen differentiation. In contrast, batches with a
 519 higher proportion of low-risk individuals yielded lower classification accuracy, in some cases
 520 dropping to as low as 72%. The reduced severity and non-specificity of symptoms in these groups
 521 likely contribute to increased classification uncertainty.

522 When examining pathogen-specific performance [Figure 5 \(subplots b, c, d\)](#), BRSV maintained an
 523 accuracy above 96% in 57% of batch configurations and exceeded 80% in 95% of cases, particularly
 524 when high- and medium-risk individuals predominated. Conversely, the *Mh* model showed an
 525 accuracy range of 88% to 94% in about 37% of cases, with higher accuracies linked to batches with
 526 predominantly high-risk individuals; its performance declined in mixed or low-risk settings, reaching
 527 between 72% and 82% in 43% of cases. *Mb* was the most challenging to classify, with overall
 528 accuracy being the lowest among the three pathogens—10% of batch configurations exhibited
 529 accuracies below 72%—particularly in batches dominated by low-risk individuals where symptom
 530 trajectories overlapped more with those of BRSV and *Mh*.

531 Overall, a clear trend emerges: classification accuracy improves with an increasing proportion of high-
 532 risk individuals, while batches with predominantly low-risk calves are more prone to
 533 misclassification. This quantitative framework offers valuable insight into the epidemiological
 534 conditions under which BRD infectious agents can be most reliably identified, highlighting the critical
 535 influence of host risk heterogeneity on diagnostic performance.

537 3.2. Economic implications of pathogen-informed treatment decisions

538 3.2.1. Profitability assessment – Expected net profit

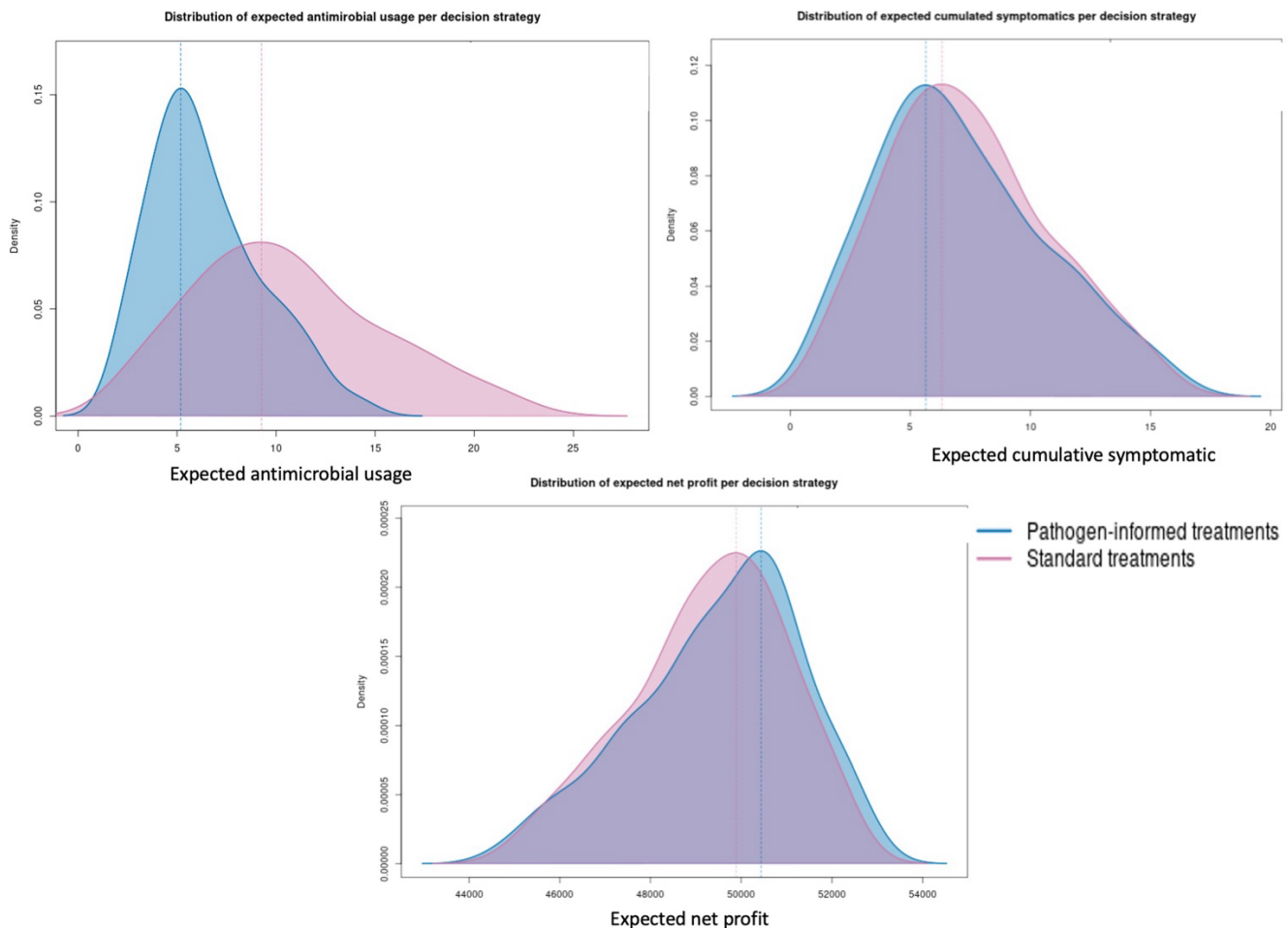


Fig 6: Pathogen informed treatment decisions versus conventional treatment decisions.

Table 6. Performance of pathogen informed treatment decision

Impact	Statistics	Conventional treatment decisions	Pathogen informed decisions
Expected net profit (K€)	Mode	49 886	50 432
	Std	1 697	1 816
Expected antimicrobial usage	Mode	9	5
	Std	4	3
Expected cumulative symptomatic	Mode	6	5.4
	Std	3	3

539

540

541

542

543

544 Results in this section present evaluation of the expected net profit of conventional treatment decisions
545 versus pathogen-informed treatment decisions (see 2.5.3 for detail).

546 The net profit is higher under pathogen-informed treatment than with conventional decisions (Figure

547 6), with a median value around 50,432 euros against 49,886 euros in the latter case – approximately
548 a 1% increase. Table 6 indicates that this approach also involves fewer antibiotic doses per batch,
549 with an average of five instead of nine (a reduction of roughly 44%), while the proportion of
550 clinically affected animals decreases marginally from to six to about 5.4 in average, a difference
551 that does not appear statistically significant (Mann-Whitney U test). The observed variability,
552 reflected in standard deviations approaching 1,800 euros for the net profit and around three to four
553 for antibiotic usage, confirms that this trend remains consistent across most simulated outbreak
554 scenarios.

555 The net profit under each strategy typically follows a moderately dispersed distribution (Figure 6),
556 with a central clustering around its respective median value and no strong skew visible in most. In
557 the pathogen-informed scenarios, the curve appears slightly widened, maybe suggesting a greater
558 variable financial outcome across different batch configurations. Regarding the antimicrobial usage,
559 the pathogen-informed curve is skewed to the lower end with a narrower distribution, suggesting a
560 consistent decrease in antimicrobial usage across different batch configurations.

561 562 4. Discussion

563 4.1. BRD infectious agent identification

564 Our theoretical investigation demonstrates that mechanistic models can effectively differentiate BRD
565 pathogens using early symptomatic data, achieving an overall classification accuracy of
566 approximately 93%. In particular, the BRSV model, with a true positive rate of 96%, clearly delineates
567 its outbreak signature from those of bacterial agents. From a modelling perspective, this high
568 performance could be a direct consequence of the properties of the discrete-time stochastic model
569 used, which rigorously captures the rapid transmission dynamics typical of airborne viruses. In
570 contrast, bacterial infections, especially those caused by *Mycoplasmopsis bovis*, present more gradual
571 and overlapping symptom patterns that result in slightly lower classification metrics. This nuance is
572 not merely an artifact of our modelling approach; it mirrors the real-world challenges faced by
573 veterinarians when diagnosing BRD, where subtle, chronic infections are notoriously difficult to
574 detect early. These outcomes are fully consistent with veterinarian knowledge; it is well established
575 that viruses like BRSV cause abrupt, pronounced clinical manifestations, whereas chronic bacterial
576 infections often yield subtler signs that complicate early diagnosis. This concordance between our
577 theoretical predictions and field observations is supported by recent studies. Moreover, the sensitivity
578 of our models to the initial risk composition of the herd - where higher proportions of high-risk
579 individuals enhance pathogen diagnostic clarity - is consistent with field data, reaffirming the critical
580 influence of batch composition on disease transmission.

581 One of the key benefits of this approach lies in its ability to distinguish cases likely caused solely by
582 BRSV from those involving bacterial pathogens. Such a distinction is crucial, as it opens the door to
583 more targeted treatment strategies, where antibiotics would not be used in cases where a viral infection
584 is strongly suspected. This advantage goes beyond economic considerations; it holds significant
585 public health implications by reducing unnecessary antibiotic consumption and mitigating the risk of
586 antimicrobial resistance.

587 However, it is important to acknowledge that these results are based on synthetic data, and although
588 the inherent stochastic variability enhances realism, validating our models against real outbreak data

589 is critical to assess their predictive reliability. Currently, there is no gold standard for evaluating
590 diseased animals based solely on visual appraisal of clinical signs, making ground truth determination
591 challenging. One promising direction for future research would be to explore how different thresholds
592 of diseased status influence the performance of pathogen identification through advanced model
593 selection methods. Optimizing the differentiation and identification accuracy of correct pathogens-
594 models (it is possible for veterinarians to biologically diagnose the nature of the infectious agents)
595 could thereby help veterinarians determine the optimal threshold of clinical signs for visual appraisal.

596 Furthermore, the mechanistic models employed in this study assume that a single pathogen dominates
597 throughout the outbreak, neglecting the possibility of co-infections or co-circulation. In reality,
598 multiple infectious agents often interact, with some pathogens acting as primary initiators and others
599 as secondary aggravators. As highlighted by Pinotti et al. (2019), such interactions can lead to non-
600 linear epidemiological patterns that complicate both diagnosis and disease management. Future
601 models should, therefore, incorporate co-infection dynamics. Extending our distinguishability method
602 to handle multi-label classification problems where an input signal may be attributed to multiple
603 pathogens with corresponding weights represents a natural and necessary progression to capture the
604 complexity of real-world outbreaks.

605 The blend of theoretical knowledge and empirical/practical veterinary knowledge could not only
606 enhance our understanding of BRD dynamics but also paves the way for developing reliable decision-
607 support tools that integrate epidemiological insights with practical treatment strategies.

608 609 4.2. *Expected profit from pathogen-tailored antibiotic treatments*

610 Results indicate that adopting a pathogen-informed decision process can provide a modest but
611 consistent financial advantage compared to conventional strategies. When using the early
612 symptomatic signals detected (5 days of observation) and mechanistic-model inference before
613 administering antibiotics, the median net profit reaches approximately 50,432 euros for a batch of 12
614 animals over the fattening period. By contrast, an empirical approach that treats all symptomatic
615 animals, irrespective of whether the pathogen is likely viral or bacterial, yields a slightly lower median
616 net profit of around 49,886 euros. Although this difference of about 546 euros represents only a
617 marginal increase of roughly one percent, the trend remains consistent across most simulated batch
618 configurations.

619 These findings also highlight a substantial decrease in antimicrobial usage, from an average of nine
620 doses per batch under the conventional protocol to about five doses under the pathogen-informed
621 strategy. This reduction, nearing forty-four percent, holds significance for both the stewardship of
622 antibiotic resources and the mitigation of antimicrobial resistance. In addition, the total number of
623 clinically affected animals across the fattening period decreases only slightly (from six to about 5.4),
624 and even though the difference in clinical outcomes does not appear statistically significant, these
625 simulations were realised with a single batch of 12 individuals, and the default probability of
626 recovering from an *Mannheimia haemolytica* infection is only 60%. Findings suggest that early,
627 model-based identification of bacterial versus viral aetiology can simultaneously preserve animal
628 welfare, improve financial benefit and substantially contribute to reducing the emergence of
629 antimicrobial resistance and save costs and time spent to buy and administer individual treatments.

630 Several limitations exist in our economic calculations. One key assumption is that all animals are

631 purchased at the same price, which does not always reflect real-world conditions. Additionally, the
632 model assumes simultaneous sale of all animals, disregarding the common practice of farmers
633 retaining those animals that have been adversely affected by disease. As such, our economic model is
634 not intended to be predictive in an absolute sense but rather serves as a framework for ranking
635 outcomes relative to each other to inform BRD control measures. Future research should aim to
636 incorporate more realistic assumptions, such as variable purchase and sale prices and dynamic
637 treatment protocols, to enhance the predictive power of the economic analysis.

638 Moreover, our study, which focuses on a single batch size of 12 animals, opens several avenues for
639 extension. In real-world settings, batch sizes vary considerably, and exploring scenarios with larger
640 or smaller populations could provide further insights into how group size influences both model
641 distinguishability and economic outcomes. Additionally, incorporating more effective or cheaper
642 control measures such as vaccination, isolation or metaphylaxis could offer a more comprehensive
643 assessment of the financial and welfare benefits, thereby refining the decision-making process for
644 BRD control.

645 Expected profitability fundamentally depends on the quality of treatment decisions taken. As
646 demonstrated by [J-S Pierre \(2023\)](#), the effectiveness of decision-making hinges not only on the
647 model's accuracy but also on the decision threshold used to determine the nature of the pathogen. In
648 our study, the decision threshold is defined as $M = \operatorname{argmax}_{m \in \mathcal{M}} P(M_i | S^*)$, meaning that the pathogen-
649 model with the highest posterior probability is the one recommended for decision-making. Exploring
650 how subtle shifts in this threshold affect profitability could reveal an optimal balance that maximizes
651 both pathogen identification and economic returns. Furthermore, our study raises the question of
652 whether a five-day observation window is optimal. Shortening this period might allow for earlier
653 interventions, but it could also compromise classification accuracy. Investigating this trade-off could
654 yield a more efficient protocol for early intervention, ensuring that initial classification translates into
655 robust long-term predictions of outbreak dynamics.

656 A key step toward building a more integrated and robust pipeline for real-world applications is the
657 explicit consideration of uncertainty. A common approach is to quantify prediction uncertainty
658 independently of its downstream impact on decision-making ([Yarin Gal et al., 2016](#); [J. Lampinen et](#)
659 [al., 2001](#); [E. Goan et al., 2018](#)). This can be achieved, for instance, by leveraging posterior
660 distributions in a Bayesian framework to construct uncertainty sets that uniformly encompass the true
661 outcomes across all predictions. The economic model can then select decisions that remain safe within
662 these uncertainty bounds. Such strategies have been successfully applied to provide safety assurances
663 ([Eyango et al., 2024](#)).

664 While our findings demonstrate the theoretical ability of mechanistic models to differentiate BRD
665 pathogens based on early symptomatic data, it is crucial to acknowledge that these results are derived
666 from simulated outbreaks. The inherent stochastic variability enhances realism, yet the models have
667 not been validated against real-world outbreak data. In practice, multiple pathogens often co-circulate,
668 and their interactions can complicate diagnosis and treatment strategies. Future research should focus
669 on empirical validation by testing these models against field data to refine their predictive power and
670 assess their robustness in real epidemiological conditions. Such validation would provide essential
671 insights into the applicability of these models as decision-support tools for veterinarians and farmers,
672 ensuring their relevance beyond controlled simulation environments.

673

674 **5. Conclusion**

675 Beyond its application to BRD, this work contributes to the broader methodological landscape of
676 model selection in epidemiology. Our approach exemplifies how to choose a statistical model that
677 aligns with real-world constraints while considering user impact. The potential application of this
678 framework extends beyond pathogen identification. Our methodology could inform the development
679 of decision-support tools that assists farmers in dynamically configuring their farm structures to
680 improve pathogen detection and/or economic efficiency. More broadly this framework provides a
681 generalizable approach for selecting the most appropriate epidemiological model based on user
682 constraints, economic considerations, and available observational data.

683 A key takeaway from this study is the importance of early decision-making. The earlier the
684 identification process is done, the sooner it can drive positive change by reducing antibiotic use,
685 improving animal welfare, and increasing economic returns (see [supplementary files](#) for results at
686 after 20 days). Given that our results demonstrate high accuracy in early pathogen identification, rapid
687 implementation is essential to maximize its impact. Furthermore, our findings suggest that our method
688 is not only efficient but also consistently outperforms empirical decision-making strategies. This
689 reinforces the idea that integrating model-based approaches into veterinary practice can elevate
690 diagnostic accuracy and enhance treatment effectiveness.

691

692

693 **Acknowledgements**

694 We extend our sincere appreciation to our colleagues from the BIOEPAR Dynamo team, particularly
695 Baptiste SORIN and Gaël BEAUNEE, for their valuable insights during the development of this work
696 and their guidance throughout the inference process. We also express our gratitude to our colleagues
697 from the Adventiel Data Science team, notably Léane GERNIGON, Bastien DELEUZE, Bastien
698 DELEUZE, Tim CRELLIN, and Leslie CIETERS, for their time and thoughtful feedback on this
699 article.

700 **Authors' contributions**

701 Conception and design of the study: LE, SP, NP. Data acquisition and analysis: LE (simulation outputs
702 and analysis). Interpretation of data: ALL. Drafting of the manuscript: LE, HF. Revisions of the
703 manuscript: ALL. All authors read and approved the final manuscript.

704

705 **Fundings**

706 This project has been financially supported by Adventiel and ANRT through CIFRE No. 2021/1805
707 and by a grant of the Carnot Institute France Futur Elevage (project SEPTIME). This Work has
708 received funding from the European Union's Horizon 2020 research and innovation programme under
709 grant agreement No. 101000494 (DECIDE). This publication only reflects the author's views and the

710 Research Executive Agency is not responsible for any use that may be made of the information it
711 contains. This work was supported by the French region Pays de la Loire (PULSAR grant) and the
712 ministry of agriculture (MultiPast grant). No funder was involved in the scientific or editorial choices
713 made for this study.

714

715 Availability of data and materials

716 Emulsion is an open-source software which can be installed as a Python module
717 (<https://sourcesup.renater.fr/www/emulsion-public>). The BRD pathogen-specific model file
718 (brd.yaml) is open-sourced and published in: <https://forgemia.inra.fr/dynamo/brd-models/brd-public>
719 in the branch “pathogen-specific-multibatch”.

720

721 References

- 722 D. Greenhalgh et M. Griffiths. Backward bifurcation, equilibrium and stability phenomena in a three-
723 stage extended BRSV epidemic model. Journal of mathematical biology, vol. 59, no 1, Art.no 1,
724 2009
- 725
- 726 S. Picault, P. Ezanno, et S. Assié. Combining early hyperthermia detection with metaphylaxis for
727 reducing antibiotics usage in newly received beef bulls at fattening operations: a
728 simulationbasedapproach. In SVEPM: Conference & Annual General Meeting, 2019, p. 148-159.
729
- 730 S. Picault, P. Ezanno, K. Smith, D. Amrine, B. White, et S. Assié. Modelling the effects of
731 antimicrobial metaphylaxis and pen size on bovine respiratory disease in high and low risk
732 fattenin cattle. Veterinary Research, vol. 53, no 1, Art. No 1, oct. 2022, doi: 10.1186/s13567-022-
733 01094-1.
- 734
- 735 S. Picault, Y.-L. Huang, V. Sicard, S. Arnoux, G. Beaun.e, et P. Ezanno. EMULSION: transparent
736 and flexible multiscale stochastic models in human, animal and plant epidemiology. PloS
737 computational biology, vol. 15, no 9, Art. No 9, 2019.
- 738
- 739 Ritchie. H., Roser. M., 2020. Meat and dairy production. Retrieved on 9 August 2020, from
740 <https://ourworldindata.org/meat-production>
- 741
- 742 Capper, J.L., Bauman, D.E., 2013. The role of productivity in improving environmental sustainability
743 of ruminant production systems. Annual Review of Animal Biosciences 1, 469–489
- 744
- 745 Babcock, A.H., White, B.J., Dritz, S.S., Thomson, D.U., Renter, D.G., et al., 2009. “Feedlot health
746 and performance effects associated with the timing of respiratory disease treatment. J. Anim. Sci.
747 87 (1), 314 –327
- 748
- 749 Bareille, Nathalie, Seegers, Henri, Quillet, Jean-Michel, Assie, Sébastien, et al., 2009. Impact of
750 respiratory disorders in young bulls during their fattening period on performance and
751 profitability. In 25. World Buiatrics Congr. 1-p

- 752
753 Mijar, Sanjaya, van der Meer, Frank, Pajor, Ed, Hodder, Abigail, Morgan Louden, Julia, Thompson,
754 Sean, Orsel, Karin, et al., 2023. Impacts of commingling preconditioned and auction-derived beef
755 calves on bovine respiratory disease related morbidity, mortality, and weight gain. *Frontiers in*
756 *Veterinary Science*, p. 10 <https://www.frontiersin.org/articles/10.3389/fvets.2023.1137078>.
757
758 Grissett, G.P., White, B.J., Larson, R.L., 2015. Structured literature review of responses of cattle to
759 viral and bacterial pathogens causing bovine respiratory disease complex. *J. Veterinary Intern.*
760 *Med.* 29 (3), 770–780. <https://doi.org/10.1111/jvim.12597>.
761
762 Théo Salles. Vers un outil d'aide à la décision : modélisation des co-infections respiratoires lors de
763 l'engraissement des jeunes bovins en France pour mieux les contrôler. *Sciences du Vivant [q-*
764 *bio]*. 2024. <https://dumas.ccsd.cnrs.fr/dumas-04919667v1>
765
766 Blakebrough-Hall C, McMeniman JP, González LA. An evaluation of the economic effects of
767 bovine respiratory disease on animal performance, carcass traits, and economic outcomes in
768 feedlot cattle defined using four BRD diagnosis methods. *J Anim Sci.* 13 janv 2020;98(2).
769
770 Assié S, Seegers H, Makoschey B, Désiré-Bousquié L, Bareille N. Exposure to pathogens and
771 incidence of respiratory disease in young bulls on their arrival at fattening operations in France.
772 *Vet Rec.* août 2009 ;165(7):195-9.
773
774 Bonnet-Beaugrand F, Poizat A, Cornette B, Duvalleix-Treguer S, Assié S, Fourichon C, et al.
775 Organisation économique de la filière française des jeunes bovins de boucherie, quelle influence
776 Sur une moindre utilisation d'antibiotiques. 2018.
777
778 Griffin, Dee, 2014. The monster we don't see: subclinical BRD in beef cattle ". *Anim. Health Res.*
779 *Rev.* 15 (2), 138–141.
780
781 Ollivett, T.L., 2020. BRD treatment failure: clinical and pathologic considerations. *Anim. Health Res.*
782 *Rev.* 21 (2), 175–176.
783
784 Ives, Samuel E., Richeson, John T., et al., 2015. Use of antimicrobial metaphylaxis for the control of
785 bovine respiratory disease in high-risk cattle (v). *Veterinary Clin. North Am. Food Anim. Pract.*
786 31 (3), 341–350. <https://doi.org/10.1016/j.cvfa.2015.05.008>.
787
788 Ives, Samuel E., Richeson, John T., et al., 2015. Use of antimicrobial metaphylaxis for the control of
789 bovine respiratory disease in high-risk cattle (v). *Veterinary Clin. North Am. Food Anim. Pract.*
790 31 (3), 341–350. <https://doi.org/10.1016/j.cvfa.2015.05.008>.
791
792 Delabouglise, A., James, A., Valarcher, J.-F., Hagglund, S., Raboissone, D., Rushton, J., 2017. Linking
793 disease epidemiology and livestock productivity: The case of bovine respiratory disease in France.
794 *PLOS ONE* 12, e0189090. <https://doi.org/10.1371/journal.pone.0189090>
795
796 Engler, M., Defoor, P., King, C., Gleghorn, J., 2014. The impact of bovine respiratory disease: the
797 current feedlot experience. *Anim. Health Res. Rev.* 15, 126–129.
798 <https://doi.org/10.1017/S1466252314000139>

- 799
800 Timsit E, Assié S, Quiniou R, Seegers H, Bareille N (2011) Early detection of bovine respiratory
801 disease in young bulls using reticulo-rumen temperature boluses. *The Veterinary Journal*
802 190:136–142. <https://doi.org/10.1016/j.tvjl.2010.09.012>
- 803
804 Kudirkiene, Egle, Aagaard, Anne Katrine, Schmidt, Louise M.B., Pansri, Potjamas, Krogh, Kenneth
805 M., Olsen, John E., et al., 2021. Occurrence of major and minor pathogens in calves diagnosed
806 with bovine respiratory disease. *Veterinary Microbiol.* 259 (août), 109135
807 <https://doi.org/10.1016/j.vetmic.2021.109135>
- 808
809 Brault, S.A., Hannon, S.J., Gow, S.P., Warr, B.N., Withell, J., Song, J., Williams, C.M., Otto, S.J.G.,
810 Booker, C.W., Morley, P.S., 2019. Antimicrobial Use on 36 Beef Feedlots in Western Canada:
811 2008–2012. *Front. Vet. Sci.* 6, 329. <https://doi.org/10.3389/fvets.2019.00329>
- 812
813 Gaudino, M., Nagamine, B., Ducatez, M.F., Meyer, G., 2022. Understanding the mechanisms of viral
814 and bacterial coinfections in bovine respiratory disease: a comprehensive literature review of
815 experimental evidence. *Vet. Res.* 53, 70. <https://doi.org/10.1186/s13567-022-01086-1>
- 816
817 Murray, G.M., More, S.J., Sammin, D., Casey, M.J., McElroy, M.C., O'Neill, R.G., Byrne, W.J.,
818 Earley, B., Clegg, T.A., Ball, H., Bell, C.J., Cassidy, J.P., 2017. Pathogens, patterns of
819 pneumonia, and epidemiologic risk factors associated with respiratory disease in recently weaned
820 cattle in Ireland. *J. Vet. Diagn. Invest.* 29, 20–34. <https://doi.org/10.1177/1040638716674757>
- 821
822 Nickell, J.S., White, B.J., 2010. Metaphylactic Antimicrobial Therapy for Bovine respiratory disease
823 in Stocker and Feedlot Cattle. *Vet. Clin. North Am. Food Anim. Pract.* 26, 285–301.
824 <https://doi.org/10.1016/j.cvfa.2010.04.006>
- 825
826 Barbara wolfger, Edouard Timsit, Bard J. White, 2015. A systematic review of bovine respiratory
827 disease diagnosis focused on diagnostic confirmation, early detection, and prediction of
828 unfavorable outcomes in feedlot cattle. DOI: 10.1016/j.cvfa.2015.05.005
- 829
830 Sébastien Picault, Guita Niang, Vianney Sicard, Baptiste Sorin-Dupont, Sébastien Assié, Pauline
831 Ezanno, 2024. Leveraging artificial intelligence and software engineering methods in
832 epidemiology for the co-creation of decision-support tools based on mechanistic
833 models. DOI: 10.1016/j.prevetmed.2024.106233
- 834
835 Véronique Bellon-Maurel, Evelyne Lutton, Pierre Bisquert, Ludovic Brossard, Stéphanie
836 Chambaron-Ginhac, Pierre Labarthe, Philippe Lagacherie, Francois Martignac, Jérôme Molenat,
837 Nicolas Parisey, Sébastien Picault, Isabelle Piot-Lepetit, Isabelle Veissier. 2022. Digital
838 revolution for the agroecological transition of food systems: A responsible research and
839 innovation perspective
- 840
841 Pauline Ezanno, Sandie Arnoux, Gael Beaunée, Hélène Cecilia. 2022. Epidemiological modelling
842 contribution to animal health.
- 843
844 S. Soubeyrand, Arnaud Estoup, Astrid Cruaud, Sylvie Malembic-Maher, Christine Meynard, et al.
845 Building integrated plant health surveillance: a proactive research agenda for anticipating and

- mitigating disease and pest emergence. CABI Agriculture and Bioscience, 2024, 5, pp.72. (10.1186/s43170-024-00273-8). <hal-04672656>
- R. Meza, K. Haaf, C. Y. Kong, A. Erdogan, W. C. Black, M. C. Tammemagi, S. E. Choi, J. Jeon, S. S. Han, V. Munshi, et al., “Comparative analysis of 5 lung cancer natural history and screening models that reproduce outcomes of the nist and plco trials,” *Cancer*, vol. 120, no. 11, pp. 1713–1724, 2014.
- E. Walter, Y. Lecourtier, and J. Happel, “On the structural output distinguishability of parametric models, and its relations with structural identifiability,” *Automatic Control, IEEE Transactions on*, vol. 29, no. 1, pp. 56–57, 1984
- Picault, S., Huang, Y.-L., Sicard, V., Arnoux, S., Beaunée, G., Ezanno, P., 2019b. EMULSION: Transparent and flexible multiscale stochastic models in human, animal and plant epidemiology. *PLOS Comput. Biol.* 15, e1007342. <https://doi.org/10.1371/journal.pcbi.1007342>.
- D. Greenhalgh et M. Griffiths. Backward bifurcation, equilibrium and stability phenomena in a three-stage extended BRSV epidemic model., *Journal of mathematical biology*, vol. 59, no 1, Art.no 1, 2009
- S. Picault, P. Ezanno, et S. Assi., Combining early hyperthermia detection with metaphylaxis for reducing antibiotics usage in newly received beef bulls at fattening operations: a simulationbasedapproach ., in SVEPM: Conference & Annual General Meeting, 2019, p. 148-159.
- S. Picault, P. Ezanno, K. Smith, D. Amrine, B. White, et S. Assié. Modelling the effects of antimicrobial metaphylaxis and pen size on bovine respiratory disease in high and low risk fattening
- N. cunniffe, Frédéric Hamelin, Abderrahman iggidr, Alin rapaport, Guathier sallet. Observability, Identifiability and Epidemiology – A survey. 2020 <https://doi.org/10.48550/arXiv.2011.12202>
- Abby Stevens, Jonathan Ozik, Kyle Chard, Jaline Gerardin, Justin M. Wozniak. 2023. NSF RESUME HPC Workshop: High-Performance Computing and Large-Scale Data Management in Service of Epidemiological Modelling. <https://doi.org/10.48550/arXiv.2308.04602>
- Pinotti, F., Ghanbarnejad, F., Hövel, P., & Poletto, C. (2019). Interplay between competitive and cooperative interactions in a three-player pathogen system
- Csilléry, K., François, O., & Blum, M. G. B. (2012). abc: an R package for approximate Bayesian computation (ABC): R package: abc. *Methods in Ecology and Evolution*, 3(3), 475–479.
- Benoteau G, Breton D, Grosbois C, Lambrecht V, Pertuisel C, Richard A, et al. Engrisseur de jeunes bovins et cultures de vente [Internet]. inosys réseaux d'élevage; 2024 [cité 14 août 2024]. Report No.: 0712T1025. Disponible sur: https://portail.inosys-reseauxelevage.fr/CasType/Filiere_2/0712T1025-2023-Edition-Cas-Type.pdf

- 893
894 CCNA [Internet]. [cité 19 juill 2024]. Mise à jour de la grille des salaires. Disponible sur :
895 <https://convention-agricole.fr/#/article/31?s=0.8953379449659475&type>
896
897 Legrand I, Tribot Laspière P, Repplinger M. Caractérisation fine des carcasses : analyse des
898 rendements selon les races, les types, les âges des bovins [Internet]. 2019 déc 3 [cité 19 juill
899 2024]; France. Disponible sur :
900 https://fr.slideshare.net/idele_institut_de_1_elevage/caractrisation-fine-des-carcasses-analysedes-rendements-selon-les-races-les-types-les-ges-des-bovins
901
902
903 Duflot B. Dossier annuel Bovins viande - Année 2023 - Perspectives 2024 [Internet]. Institut de
904 l'élevage; 2024 févr [cité 11 avr 2024]. Report No.: 546. Disponible sur :
905 <https://idele.fr/detailarticle/dossier-annuel-bovins-viande-annee-2023-perspectives-2024>
906
907 Kurucay, H. N., Yazici, Z., & Bayrakal, V. (2025). *A surrogate in vitro experimental model for off-label drug repurposing : inhibitory effect of montelukast on bovine respiratory syncytial virus replication*. Virology Journal.
908
909
910 Mohamed, R. A., & Abdelsalam, E. B. (2008). *A review on pneumonic pasteurellosis (respiratory mannheimiosis) with emphasis on pathogenesis, virulence mechanisms, and predisposing factors*. ResearchGate.
911
912
913
914 Bürki, S., Frey, J., & Pilo, P. (2015). *Virulence, persistence and dissemination of Mycoplasma bovis*. Veterinary Microbiology, 179(1-2), 70-78.
915
916
917 Maunsell, F. P., & Donovan, G. A. (2009). *Mycoplasma bovis infections in young calves*. Veterinary Clinics : Food Animal Practice, 25(1), 139-177
918
919
920 Wang M, Schneider LG, Hubbard KJ, Grotelueschen DM, Daly RF, Stokka GS, et al. Beef producer
921 survey of the cost to prevent and treat bovine respiratory disease in preweaned calves. J Am Vet
922 Med Assoc. 1 sept 2018 ;253(5):617-23.
923
924 Y. Gal and Z. Ghahramani, “Dropout as a Bayesian approximation: Representing model uncertainty
925 in deep learning,” in International Conference on Machine Learning. PMLR, 2016, pp. 1050–
926 1059.
927
928 J. Lampinen and A. Vehtari, “Bayesian approach for neural networks—review and case studies,”
929 Neural networks, vol. 14, no. 3, pp. 257–274, 2001.
930
931 E. Goan and C. Fookes, “Bayesian neural networks: An introduction and survey,” Case Studies in
932 Applied Bayesian Data Science: CIRM Jean-Morlet Chair, Fall 2018, pp. 45–87, 2020.
933
934 Theophile Ghislain Loic Eyango Tabi, Maud Rouault, Victoria Potdevin, Xavier L'hostis, Sébastien
935 Assié, et al.. Harnessing uncertainty: a deep mechanistic approach for cautious diagnostic and
936 forecast of Bovine Respiratory Disease. Preventive Veterinary Medicine, 2024, 233, pp.106354.
937 10.1016/j.prevetmed.2024.106354
938
939